Spring 2020

Galvanic Corrosion in Aluminum/Steel Joints

Maegan Saul
mes188@zips.uakron.edu

Galvanic Corrosion in Aluminum/Steel Joints

Maegan Saul

Department of Corrosion Engineering

Honors Research Project

Submitted to

The Williams Honors College
The University of Akron

Approved:

Dr. David M. Bastidas

Date: 5/15/2020
Honors Project Sponsor (signed)

David M. Bastidas
Honors Project Sponsor (printed)

Dr. Scott Lillard

Date: 5/18/2020
Reader (signed)

Scott Lillard
Reader (printed)

Dr. Rajeev Gupta

Accepted:

Dr. Hongbo Cong

Date: 5/18/2020
Honors Department Advisor (signed)

Hongbo Cong
Honors Department Advisor (printed)

Dr. Michael Cheung

Date: 5/18/2020
Department Chair (signed)

Michael Cheung
Department Chair (printed)

Date: 5/18/2020
Reader (signed)

Rajeev Gupta
Reader (printed)

Galvanic Corrosion in Aluminum/Steel Joints

4250:497-003

Maegan Saul

Sponsor: Prof. David M. Bastidas

Co-advisor: Eng. Juan Bosch

April 24th, 2020

Table of Contents

Executive Summary

Galvanic corrosion has become significantly more of a problem in society as goals of creating more lightweight, efficient, and emissions-friendly vehicles leads to the pairing of lightweight aluminum alloys with structural carbon steel frames. There is a need for better understanding the corrosion behavior of this metallic coupling in various environments so that safer structures can be made. In this study, Carbon Steel (CS) and two Aluminum Alloys (AA1 and AA2) were first characterized for their individual corrosion behavior. Potendiodynamic polarization curves were obtained for each metal, and electrochemical impedance spectroscopy (EIS) was also performed. These tests were all run using a rotating disk electrode (RDE) at various speeds (0, 100, 500, 1000, and 2000 rpm) immersed in both 0.06M NaCl solution and 0.6M NaCl solution. The Nyqiust plots generated from the EIS data formed no clear trends. Results from the polarization tests suggest that, to varying degrees for each metal, corrosion is more aggressive as the electrolyte layer becomes thinner (as the RDE speed increases). To characterize the galvanic corrosion behavior of the metal couples, zero resistance ammeter (ZRA) tests were then run on joints of CS + AA1 and CS + AA2 in 0.6M NaCl solution. Besides the first test run of CS + AA1, the galvanic coupling current of all of the other tests was nearly the same at approximately -1×10^{-11} A/cm^2. Due to the COVID-19 situation, no further testing was completed. Additional parameters are needed before a comprehensive mathematical model/simulation can be produced, which leads to many ideas as to which direction to go for potential future work on the project.

Introduction

As automotive manufacturers push towards new and more efficient technology utilizing the power of electric motors and batteries, they are faced with a challenge of using lighter weight structural materials to offset the heavier weight of the batteries or reduce the greenhouse emissions. One promising metal to use is aluminum, which exhibits the necessary light weight properties and is available in many different alloy compositions for specific service requirements. A problem arises when two dissimilar metals, such as aluminum and carbon steel, are connected together in a structure. The difference in the potentials of the two metals creates a galvanic couple between them, leading to the anodic dissolution of the metal with lesser nobility. Eventually the part is subject to fail as its structural integrity will be negatively affected over time, the rate by which is controlled by how aggressive the environment is. Experimental testing can be used to model and predict the corrosion process of a galvanic couple in dissimilar metal joints under atmospheric corrosion conditions, lending to a better understanding of the electrochemical behavior of galvanic couples. Using this knowledge, better informed decisions can be made regarding mitigation strategies to decrease the destructive influence of galvanic coupling in dissimilar metal joints, leading to safer and improved structures being developed in society. Better industry understanding of the issues at hand can also result in more effective programs for corrosion management and mitigation.

Background

When two dissimilar metals with different potentials are coupled together in an environment that allows for the flow of ions and electrons, a galvanic cell has been created. Oxidation reactions happen at the less noble metal, or the anode. Reduction reactions happen at the more noble metal, or the cathode. An example of a galvanic cell can be seen below in **Figure 1**.

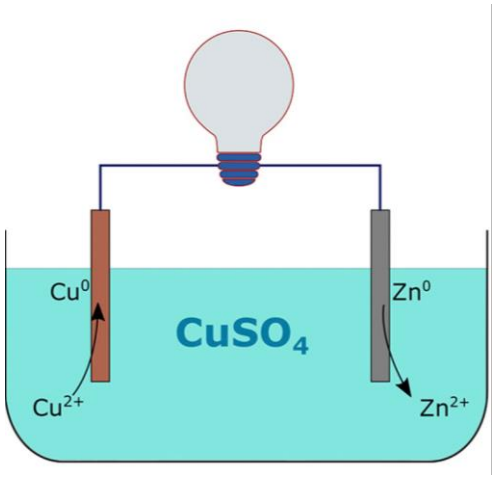

Figure 1. Example of a galvanic cell between Cu and Zn [1].

As pictured above in **Figure 1**, Zn metal oxidizes to Zn^{2+} ions (anode) and Cu^{2+} ions reduce to Cu metal (cathode) when coupled together in a solution with an electron path. In this cell, Zn is actively corroding since it is less noble than Cu (which is based-off of the standard reduction potential of each metal).

One way to characterize the corrosion behavior of metals is through electrochemical testing. A potentiodynamic polarization curve (PPC) is obtained by constructing a cell that includes a working electrode (the metal to be observed), a reference electrode, and a counter electrode in a particular solution (often, some concentration of NaCl in DI water) hooked up to a potentiostat. The sample is then polarized above and below its open circuit potential over a specified potential range (i.e., +/- 800 mV). As this change in voltage occurs, the response in current is measured which results in a graph of *E* (potential) vs. *i* (current density) [2]. An example of a PPC can be seen below in **Figure 2**.

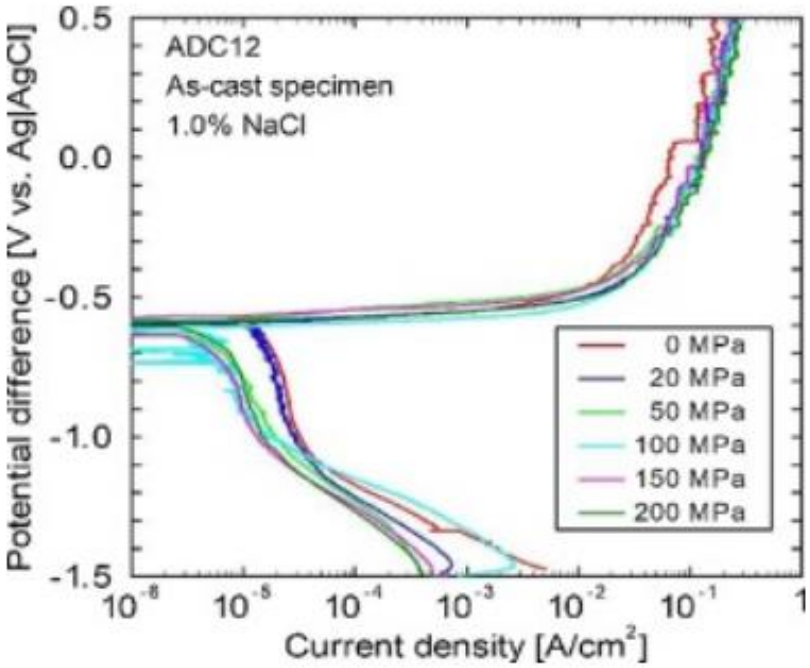

Figure 2. Polarization curve of a cast aluminum alloy subjected to various stress in a sodium chloride solution [2].

The top half of the curve is the anodic portion and the bottom half is the cathodic portion. Tangential lines can be drawn along both the anodic and cathodic branches of the curve. At the point where the lines intersect, the potential read to the left is the corrosion potential (E_{corr}) and the current density read to the bottom is the corrosion current density (i_{corr}). The i_{corr} value is directly proportional to the corrosion rate, which can be calculated using the following equation, (**Eq. 1**):

$$CR\ (mpy) = \frac{0.129 \times i_{corr} \times EW}{\rho} \quad (1)$$

where i_{corr} is the corrosion current density (μA/cm^2), EW is the equivalent weight of the material (g/equiv), and ρ is the density of the material (g/cm^3).

Electrochemical impedance spectroscopy (EIS) is another method of electrochemical testing. A small AC potential is applied to the cell and the response in current is recorded. This method can be used to analyze metals, oxide films, and even coatings. EIS provides a way to characterize the cell by determining its equivalent electrical circuit, therefore better describing the

mechanism of what is occurring. Furthermore, it is a nondestructive technique which increases its utility.

As the name suggests, EIS uses impedance as a function of the potential and current. When a sinusoidal potential is applied, the current will respond with sinusoidal behavior of the same frequency but with a shift in phase. The radial frequency is characterized by the equation, (**Eq. 2**):

$$\omega = 2 \times \pi \times f \tag{2}$$

where f is the frequency in Hz. The potential and current behaviors are characterized by the equations (**Eqs. 3,4**):

$$E_t = E_0 \times \sin(\omega t) \tag{3}$$

$$I_t = I_0 \times \sin(\omega t + \theta) \tag{4}$$

where E_t is the potential at time t, E_0 is the signal amplitude, ω is the radial frequency, I_t is the response signal shifted in phase θ, and I_0 is the amplitude. Based on this, the relationship to impedance can be calculated, (see **Eq. 5**):

$$Z = \frac{E_t}{I_t} = \frac{E_0 \times \sin(\omega t)}{I_0 \times \sin(\omega t + \theta)} = Z_0 \frac{\sin(\omega t)}{\sin(\omega t + \theta)} \tag{5}$$

and following Euler's relationship (see **Eq. 6**):

$$\exp(j\theta) = \cos(\theta) + j\sin(\theta) \tag{6}$$

gives the following for impedance expressed as a complex number (see **Eq. 7**):

$$Z(\omega) = \frac{E}{I} = Z_0 \exp(j\theta) = Z_0(\cos\theta + j\sin\theta) \tag{7}$$

which is useful for interpretation of the involved mechanism [3].

The resulting data can be plotted on a Nyquist (–Z'' [imaginary] vs Z' [real]) plot and a Bode plot (|Z| and phase angle vs frequency). Examples of these two plots can be seen below in **Figure 3**.

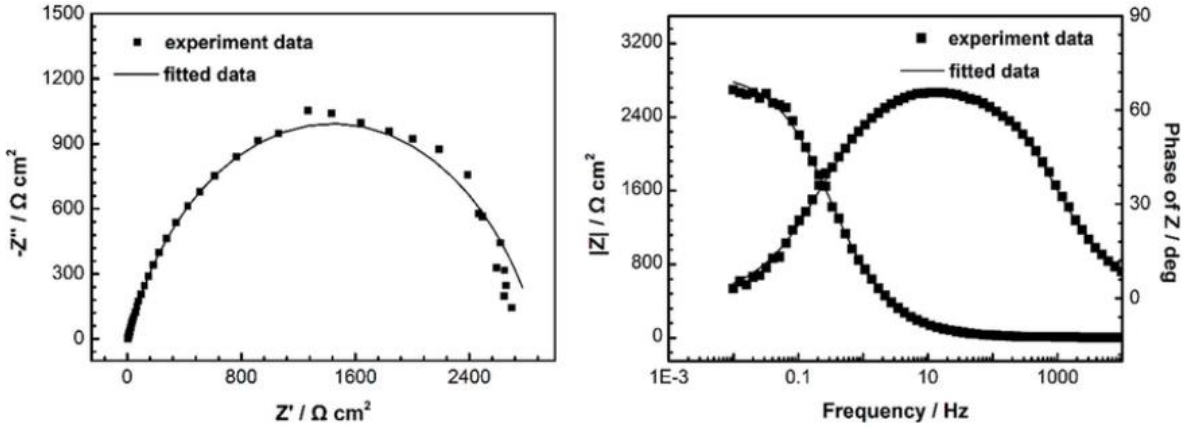

Figure 3. Example Nyquist and Bode plots of EIS data collected on steel in seawater [4].

This data can be used to approximate an equivalent electrical circuit which explains the electrochemical behaviors of the created cell. Both resistance and capacitance can be taken into account, generating a comprehensive picture of the corrosion mechanism, coating effectiveness, etc. Examples of equivalent circuits can be seen below in **Figure 4**.

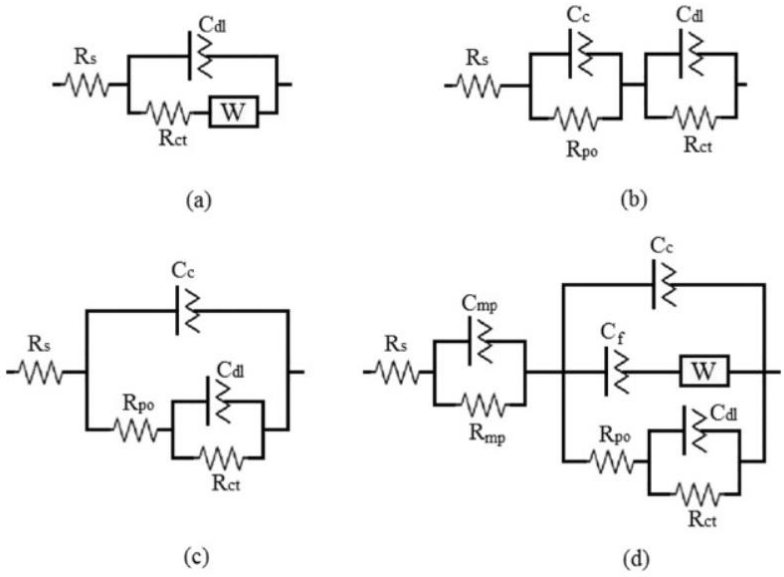

Figure 4. Examples of possible equivalent circuits described by EIS results [5].

Both PPC and EIS techniques can be run using a rotating disk electrode (RDE) which adds an element to the cell by allowing the working electrode to rotate at a specified rate. This allows for an alternation of the boundary layer thickness of the electrolyte on the electrode and can be used to simulate different environments. Low speeds are more similar to immersion while fast speeds simulate less moisture on the surface of the material (humid environment, condensation) [6].

In order to model the flow and diffusion parameters when using a rotating disk electrode, a new equation is needed. Thus, comes the Levich equation (see **Eq. 8**):

$$I_L = (0.201) \times n \times F \times A \times D^{\frac{2}{3}} \times \omega^{\frac{1}{2}} \times \vartheta^{\frac{-1}{6}} \times C \quad (8)$$

where I_L is the Levich, or limiting, current (A), n is the number of moles of electrons transferred, F is the Faraday constant (C/mol), A is the area of the electrode (cm^2), D is the diffusion coefficient (cm^2/s), ω is the angular rotation (rpm), v is the kinematic viscosity (cm^2/s), and C is the concentration of the analyte (mol/cm^3).

Plugging in the values of the experimental setup allows for a diffusion coefficient to be calculated for the material in its particular environment. This allows for further insight into the behavior by which it is corroding in solution.

While those two methods are vital for characterizing the detailed behavior of a single material in a particular environment, another method is needed to characterize the behavior of a galvanic coupling of metals. One such way to accomplish this is to use a zero-resistance ammeter (ZRA).

ZRA allows for two dissimilar metals to be placed in the same electrolyte and the resulting galvanic potential and current flowing between the materials to be monitored. For this setup, two working electrodes are needed to create the galvanic coupling necessary to produce the required results. Once all of the data is compiled, comparisons can be made with the galvanic potentials and currents of different pairings of metals in different environments [7].

Experimental Methods

Samples of carbon steel (CS) and two aluminum alloys (referred to as AA1 and AA2) were cut to shape for use as rotating disk electrodes with areas of 2.88 cm^2. Solutions of 0.06M and 0.6M NaCl were prepared.

Before each electrochemical test, the samples were successively polished with 240, 600, and 1200 grit SiC polishing paper. This was followed by an ethanol rinse to clean the pieces.

For each test, the samples were mounted onto the RDE apparatus and lowered into the appropriate NaCl solution with a three-electrode cell configuration. A silver-silver chloride electrode (SSC) was used as the reference electrode and a graphite rod as a counter electrode (CE). The material being studied was the working electrode (WE). EC-lab software was used to input, run, and monitor each electrochemical test.

Potentiodynamic polarization tests were run on the CS, AA1, and AA2 samples at 0, 100, 500, 1000, and 2000 rpm in both the 0.06M and 0.6M NaCl solutions. Before the start of each test, the open circuit potential was allowed to stabilize for a duration of one hour, followed by the polarization test and the EIS. Settings for the polarization test included a scan range of ±800 mV, scan rate of 2 mV/s, and sample period of 2 s. These settings are summarized below in **Table 1**.

Table 1. Summary of potentiodynamic polarization test parameters.

POTENTIODYNAMIC POLARIZATION TESTS

METALS	CS, AA1, and AA2
RDE SPEED	0, 100, 500, 100, and 2000 rpm
NACL SOLUTION CONCENTRATION	0.06M and 0.6M
OCP STABILIZATION DURATION	1 hr
SCAN RANGE	±800 mV
SCAN RATE	2 mV/s
SAMPLE PERIOD	2 s

Electrochemical impedance spectroscopy (EIS) tests were also run on the CS, AA1, and AA2 samples at 0, 100, 500, 1000, and 2000 rpm in both the 0.06M and 0.6M NaCl solutions. Settings for the test included a frequency of 1-10 MHz, potential of 10 mV (rms), and 10 steps/decade. These settings are summarized below in **Table 2**.

Table 2. Summary of EIS test parameters.

EIS TESTS	
METALS	CS, AA1, and AA2
RDE SPEED	0, 100, 500, 1000, and 2000
NACL SOLUTION CONCENTRATION	0.06M and 0.6M
FREQUENCY	1-10 MHz
POTENTIAL	10 mV
STEPS/DECADE	10

To characterize the galvanic corrosion behavior of the coupled metals, zero resistance ammeter (ZRA) tests were also completed. The setup in this case changed; the WE and the CE were both materials being studied and the RE remained the same. The areas for each metal sample were approximated to be 1 cm^2. These settings are summarized below in **Table 3**.

Table 3. Summary of ZRA test parameters.

ZRA TESTS	
METALS	CS + AA1 and CS + AA2
NACL SOLUTION CONCENTRATION	0.6M
RUN TIME	10800 s
LIMIT *I*	100 mA/cm^2

Upon 3 hours of exposure in the 0.6M NaCl solution, an optical microscope was used to obtain images of the test specimen surfaces from the ZRA tests. Magnification ranged from ×1 to ×3.

Results and Discussion

To study the general corrosion behavior of each metal, individual potentiodynamic polarization and EIS tests were first run with varying electrode speeds in different NaCl solution concentrations.

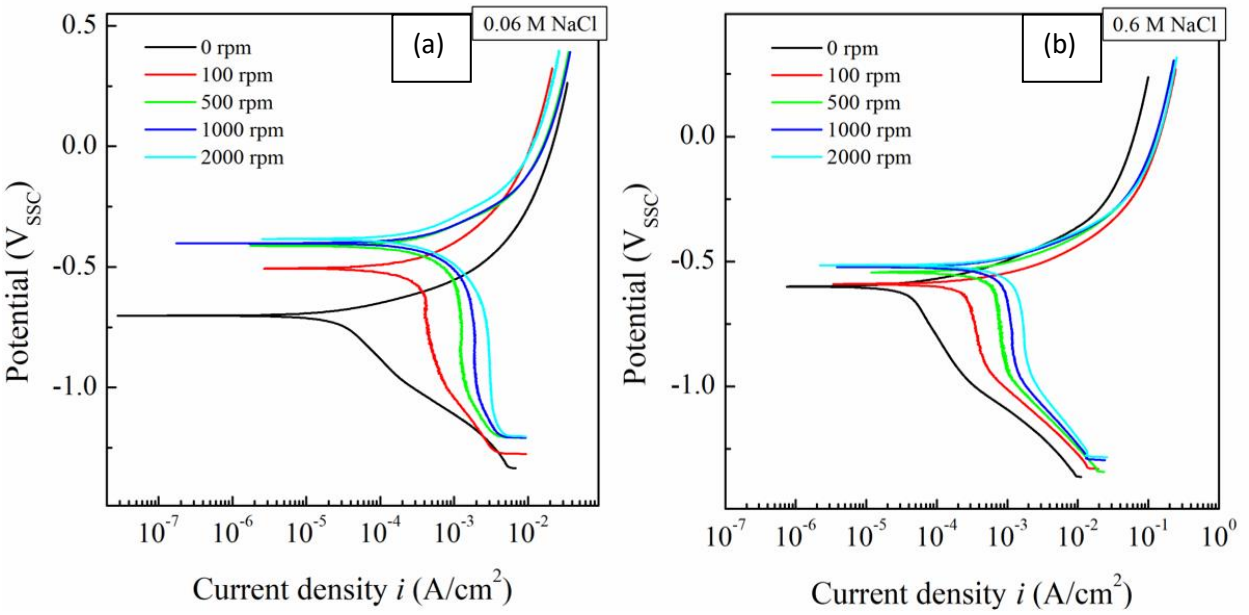

Figure 5. PCCs of Carbon Steel in (a) 0.06M NaCl and (b) 0.6M NaCl at 0, 100, 500, 1000, and 2000 rpm.

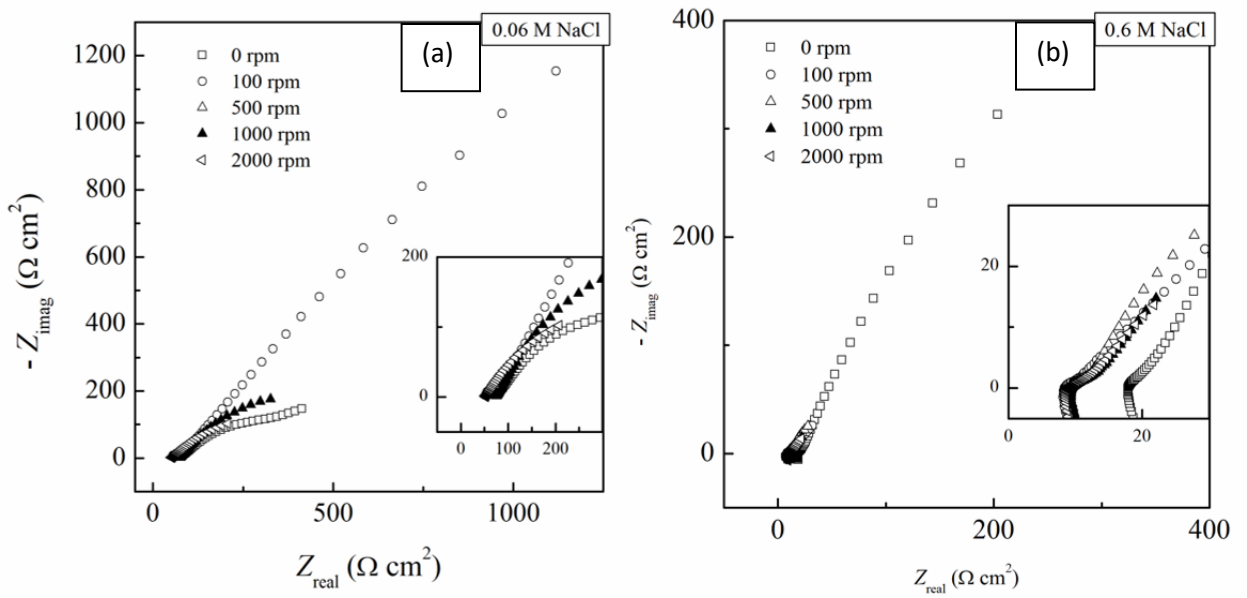

Figure 6. EIS graphs (Nyquist plots) of Carbon Steel in (a) 0.06M NaCl and (b) 0.6M NaCl at 0, 100, 500, 1000, and 2000 rpm.

The polarization and EIS graphs for Carbon Steel can be seen above in **Figures 5-6**. For **Figure 5**, in both 0.06M and 0.6M NaCl solutions, the corrosion potential (E_{corr}) increases along with an increase in rotation speed of the rotating disk electrode. This is more pronounced in the 0.06M NaCl solution. A similar trend is also seen with the corrosion current density (i_{corr}) increasing along with rotation speed as well, except in both solutions the curves for 500, 1000, and 2000 rpm are very similar in shape and i_{corr}. This is directly proportional to the corrosion rate of the metal in solution. **Figure 6** displays Nyquist plots for the two NaCl solutions at varying rotational speeds. No clear trends can be seen among the charts, but the shapes of the curves for 100 rpm in 0.06M NaCl and 0 rpm in 0.6M NaCl seem to be vastly different.

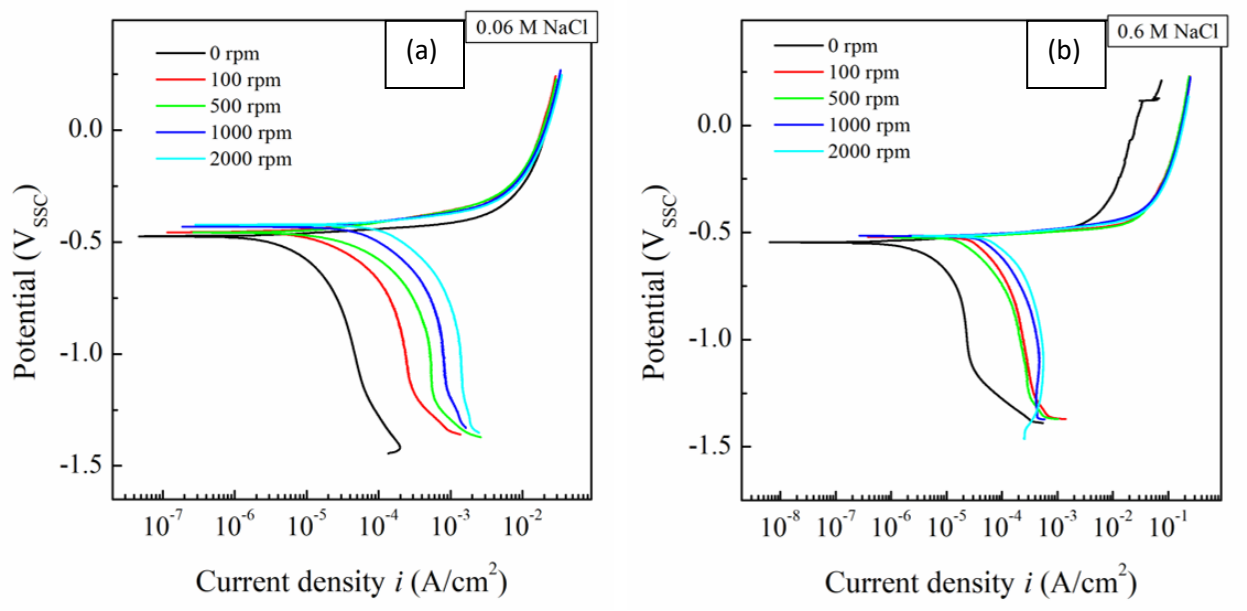

Figure 7. PCCs of AA1 in (a) 0.06M NaCl and (b) 0.6M NaCl at 0, 100, 500, 1000, and 2000 rpm.

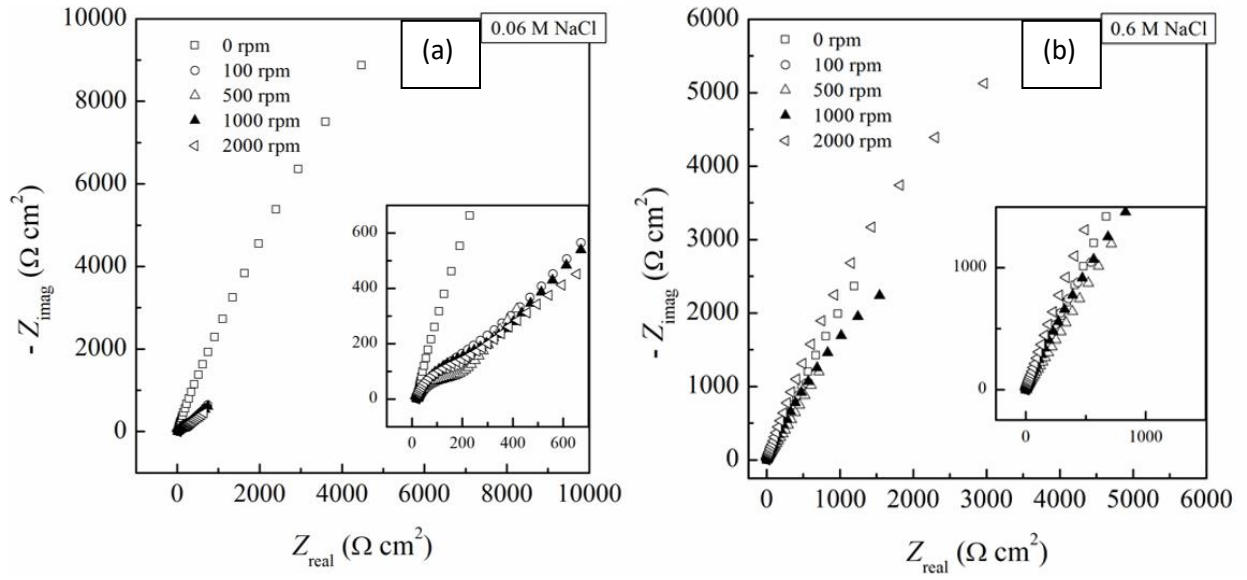

Figure 8. EIS graphs (Nyquist plots) of AA1 in (a) 0.06M NaCl and (b) 0.6M NaCl at 0, 100, 500, 1000, and 2000 rpm.

The polarization and EIS graphs for Aluminum Alloy 1 can be seen above in **Figures 7-8**. Unlike with the Carbon Steel, for AA1 in both NaCl solution concentrations there is not much

change in the E_{corr} values. In 0.06M NaCl, an increase in i_{corr} (and therefore, corrosion rate) can be seen with increasing rotational speed of the electrode. In 0.6M NaCl, the graphs are nearly identical with the exception of 0 rpm. The Nyquist plots in **Figure 8** show little differentiation between speeds. No clear trends can be seen, but the shapes of the curves for 0 rpm in 0.06M NaCl and 2000 rpm in 0.6M seem to be different from the cluster of the rest.

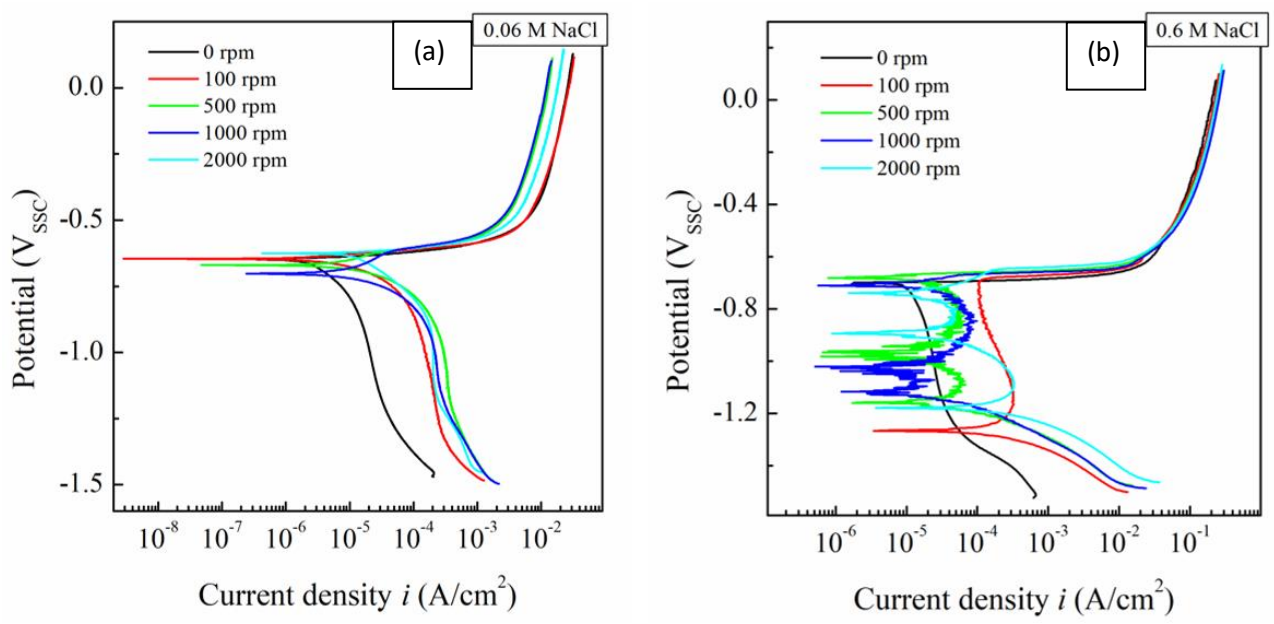

Figure 9. PCCs of AA2 in (a) 0.06M NaCl and (b) 0.6M NaCl at 0, 100, 500, 1000, and 2000 rpm.

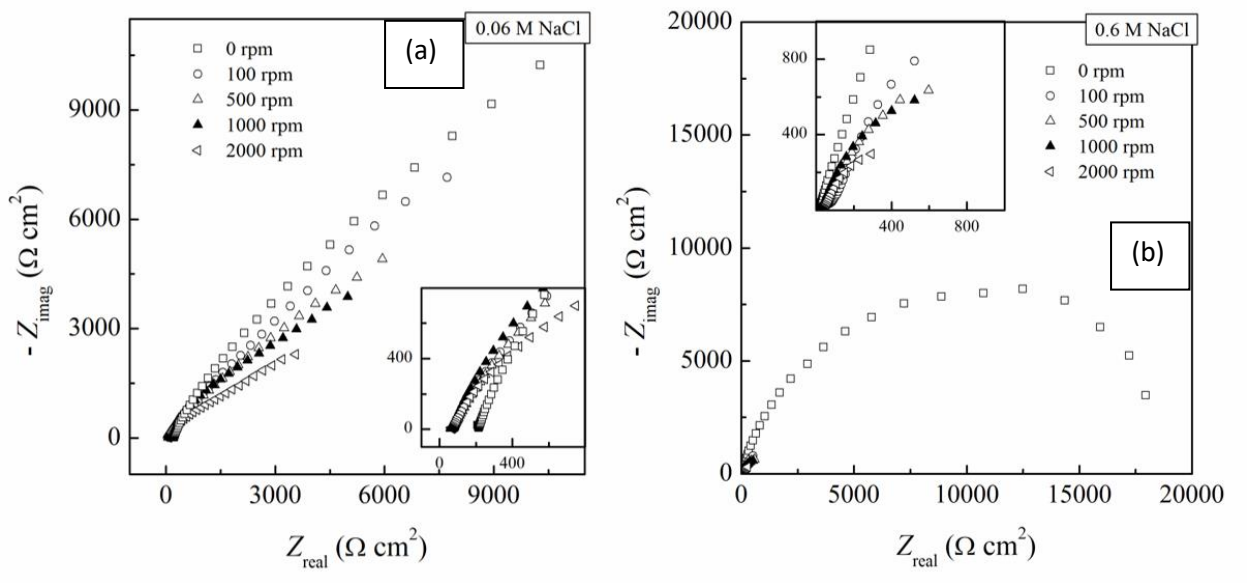

Figure 10. EIS graphs (Nyquist plots) of AA2 in (a) 0.06M NaCl and (b) 0.6M NaCl at 0, 100, 500, 1000, and 2000 rpm.

The polarization and EIS graphs for Aluminum Alloy 2 can be seen above in **Figures 9-10**. As seen in **Figure 9**, for AA2 in 0.06M NaCl, there does not seem to be a trend for changes in rotational speed clearly affecting E_{corr} and i_{corr}; the curves are fairly clustered together. There is significant noise seen in the 500 rpm and 1000 rpm curves in 0.6M NaCl. This makes it difficult to distinguish any clear trends. These tests should be repeated but due to the current COVID-19 situation, it was not possible to complete this. As for the Nyquist plots in **Figure 10**, the curves look very similar in 0.06M NaCl. In 0.6M NaCl, the 0 rpm curve is the first to display the semi-circle that is indicative of corrosion occurring.

In order to exhibit the galvanic corrosion behavior of the coupled metals, ZRA tests were run on a pairing of carbon steel with each of the aluminum alloys in 0.6M NaCl solution.

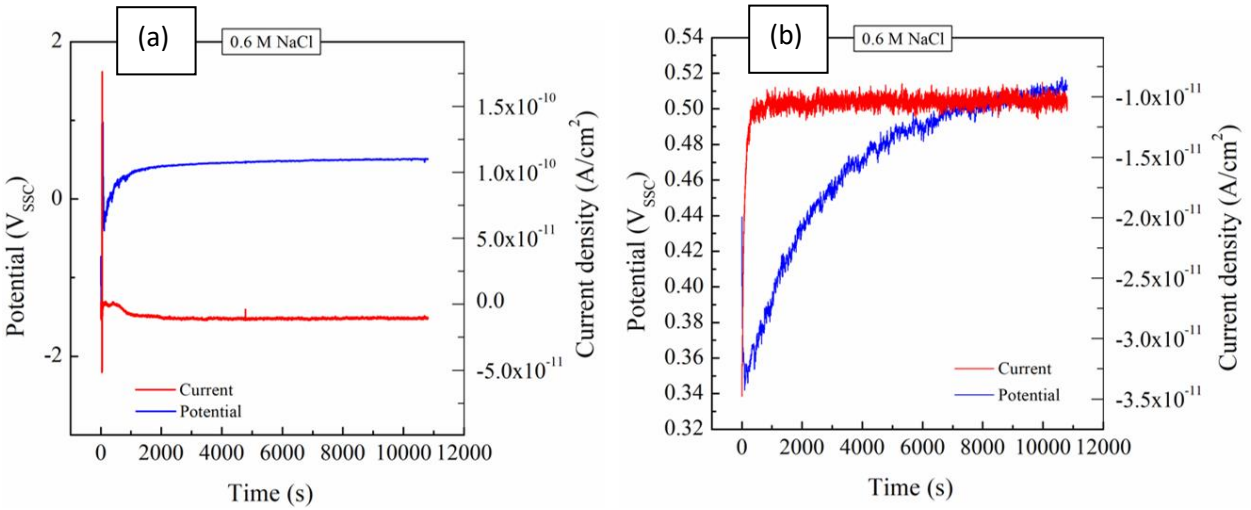

Figure 11. Graphs from ZRA test of Carbon Steel and AA1 (a) run 1 and (b) run 2 as shown by plotting potential and current density over time.

The change in potential and current density over time for two ZRA test runs of Carbon Steel paired with Aluminum Alloy 1 can be seen above in **Figure 11**. In the first test run, the galvanic coupling current density is slightly less than 0 A/cm^2 while in the second run it is approximately -1×10^{-11} A/cm^2. This low current indicates that the galvanic couple is not apparent. However, literature shows that galvanic corrosion should be expected. For this reason, these experiments should be revisited and redesigned.

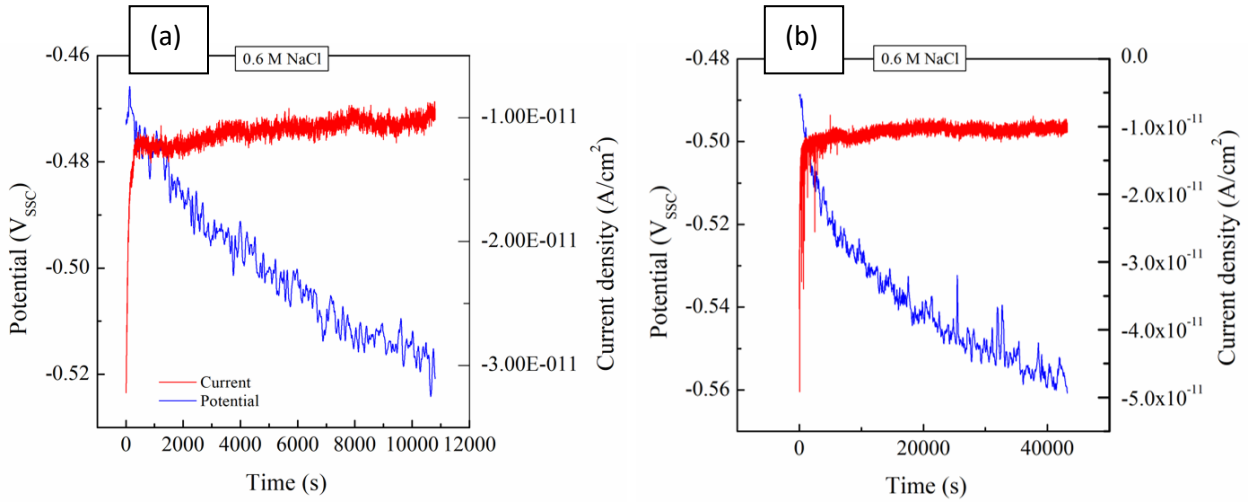

Figure 12. Graphs from ZRA test of Carbon Steel and AA2 (a) run 1 and (b) run 2 as shown by plotting potential and current density over time.

The two ZRA tests of Carbon Steel paired with Aluminum Alloy 2 can be seen above in **Figure 12**. Both test runs consistently show a galvanic coupling current density of approximately -1×10^{-11} A/cm^2. This is nearly identical to that of the second test run of Carbon Steel with AA1.

After 3 hours of 0.6M NaCl solution exposure, the ZRA test specimens were placed under an optical microscope for analysis.

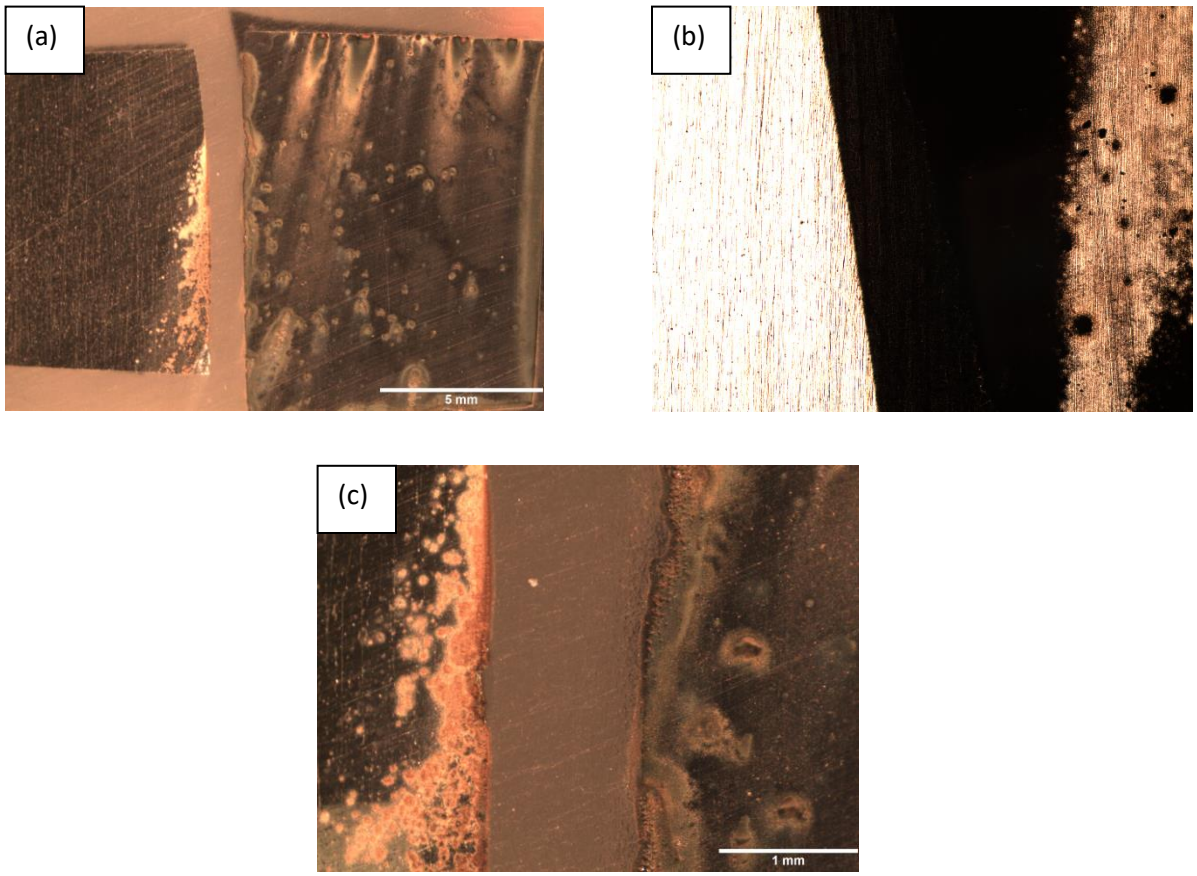

Figure 13. Optical microscope images of AA1 (left) and Carbon Steel (right) from ZRA tests pictured at (a) ×0.67, (b) ×2.5, and (c) ×3 magnification.

As seen above in **Figure 13**, there is corrosion seen on both the aluminum and carbon steel samples from the ZRA test. This is due to the coupling of the dissimilar metals for a prolonged period of time in a NaCl solution which allowed galvanic corrosion to occur. This corrosion was monitored using the ZRA, though the results were not as expected. Since the optical microscope images show the effects of galvanic corrosion, the electrochemical test should be revisited in order to clarify this behavior.

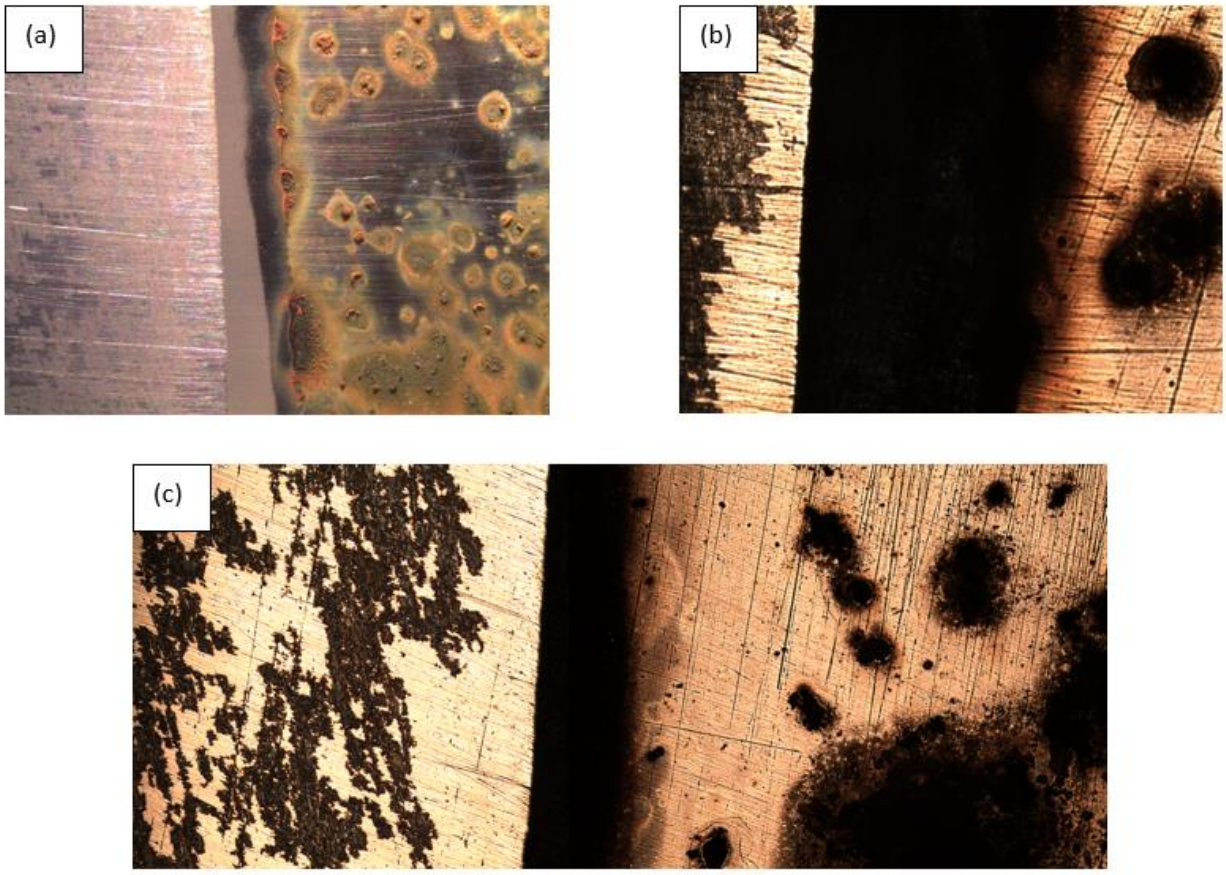

Figure 14. Optical microscope images of AA2 (left) and Carbon Steel (right) from ZRA tests pictured at (a) ×1, (b) ×2.5, and (c) ×2.5 magnification.

Similar to **Figure 13**, the images in **Figure 14** also depict up close the corrosion that has occurred on the surface of the carbon steel and aluminum coupons due to immersion together in salt solution for a prolonged period of time.

Conclusion

Based on the results from the study, Carbon Steel showed the most variance in E_{corr} and i_{corr} when the rotational speed of the rotating disk electrode was changed for both 0.06M and 0.6M NaCl solutions. Both Aluminum Alloy 1 and Aluminum Alloy 2, however, showed only mild changes in i_{corr} and almost no discernable changes in E_{corr} as rotational speed increased. In varying degrees of severity, though, it appears that i_{corr} (and therefore, corrosion) increases as the electrolyte layer becomes thinner with increasing rotational speeds. This also promotes the oxygen diffusion and increasing the available oxygen in turn increases the corrosion rate.

Most of the trends in the Nyquist plots did not seem to indicate corrosion occurring except for Aluminum Alloy 2 at 0 rpm in 0.6M NaCl, which did display the characteristic semi-circle indicative of the corrosion process. Disregarding the first ZRA test of Carbon Steel and Aluminum Alloy 1, the other tests all yielded the same galvanic coupling current density of approximately -1×10^{-11} A/cm^2.

In order to more comprehensively characterize the galvanic corrosion behavior of the coupled metals, additional tests should be run. Due to the COVID-19 situation, however, additional data was not able to be collected because of campus closure. Because of this, the project remains ongoing. There are a plethora of options for potential future work based on other studies seeking to model galvanic coupling behavior. One method involves using Scanning Vibrating Electrode Technique (SVET) to measure the distribution of current density over the coupled surface, providing more detailed information on the flow of ions over the sample [8-13]. SVET can also be used in conjunction with fibre optics micro-optode, which monitors dissolved oxygen levels; this is important because monitoring the oxygen reduction reaction in situations (neutral and alkaline solutions) where it is the cathodic process helps to further provide more detailed information for a reaction that governs the corrosion process [8, 10, 14-17]. Another important aspect to consider when generating comprehensive data for a mathematical galvanic corrosion model is to monitor local changes in pH, which can be done with a pH sensitive glass capillary micro-electrode [8, 18-21]. The combination of all of these three techniques plus the data that has already been acquired would hopefully provide adequate information for producing a model simulation of the galvanic corrosion process.

With additional, comprehensive data collected surrounding multiple aspects of the galvanic corrosion coupling, a mathematical model/simulation could then be prepared. A typical way of producing these models and simulations for galvanic corrosion is to use finite element methods (FEM) [8, 22-26]. The resulting model could then be used to predict the galvanic corrosion behavior in varied environments, providing a useful tool to industries where these metal couplings have become more common.

Acknowledgements

This work would not have been possible without the facilities provided by The University of Akron and the NCERCAMP. I would like to extend special thanks to Dr. David M. Bastidas and Juan Bosch for their continued hard work, support, and feedback necessary to produce this project.

References

[1] Karel L, Jakub S, Petr S, Petr V. (2018). Boosting of the Output Voltage of a Galvanic Cell. *Electrochimica Acta 282*(1): 331-335.

[2] Kuwazaru O, Ode K, Yamada M, Kassab A, Divo E. (2018). Experimental and Boundary Element Method Study on the Effect of Stress on the Polarization Curve of Cast Aluminum Alloy in Sodium Chloride Solution. *Corrosion Science 132*(1): 136-145.

[3] Diego L. Performance Analysis of 3D Printed 718 Alloy for Corrosive Environments. (2015). Master's Dissertation – The University of Manchester.

[4] Feng P, Wan K, Cai G, Yang L, Li Y. (2017). Synergistic Protective Effect of Carboxymethyl Chitosan and Cathodic Protection of X70 Pipeline Steel in Seawater. *RSC Advances 7*(6): 3419-3427.

[5] Arabzadeh H, Shahidi M, Foroughi MM. (2017). Electrodeposited Polypyrrole Coatings on Mild Steel: Modeling the EIS Data with a New Equivalent Circuit and the Influence of Scan Rate and Cycle Number on the Corrosion Protection. *Journal of Electroanalytical Chemistry 807*(1): 162-173.

[6] Cheng, F.y. "Erosion-Accelerated Corrosion in Flow Systems: the Behavior of Aluminum Alloys in Automotive Cooling Systems." *Tribocorrosion of Passive Metals and Coatings*, 2011, doi:10.1533/9780857093738.3.475.

[7] Espallargas N, Johnsen R, Torres C, Munoz AI. (2013). A New Experimental Technique for Quantifying the Galvanic Coupling Effects on Stainless Steel During Tribocorrosion Under Equilibrium Conditions. *Wear 307*(1-2): 190-197.

[8] Snihirova, Darya, et al. "Galvanic Corrosion of Ti6Al4V -AA2024 Joints in Aircraft Environment: Modelling and Experimental Validation." *Corrosion Science*, vol. 157, 2019, pp. 70–78., doi:10.1016/j.corsci.2019.04.036.

[9] Coelho, L.b., et al. "A SVET Study of the Inhibitive Effects of Benzotriazole and Cerium Chloride Solely and Combined on an Aluminium/Copper Galvanic Coupling Model." *Corrosion Science*, vol. 110, 2016, pp. 143–156., doi:10.1016/j.corsci.2016.04.036.

[10] Snihirova, Darya, et al. “Corrosion Inhibition Synergies on a Model Al-Cu-Mg Sample Studied by Localized Scanning Electrochemical Techniques.” *Corrosion Science*, vol. 112, 2016, pp. 408–417., doi:10.1016/j.corsci.2016.08.008.

[11] Shi, Hongwei, et al. “Simulating Corrosion of Al2CuMg Phase by Measuring Ionic Currents, Chloride Concentration and PH.” *Corrosion Science*, vol. 88, 2014, pp. 178–186., doi:10.1016/j.corsci.2014.07.021.

[12] Bastos, A. C., et al. “Review—On the Application of the Scanning Vibrating Electrode Technique (SVET) to Corrosion Research.” *Journal of The Electrochemical Society*, vol. 164, no. 14, 2017, doi:10.1149/2.0431714jes.

[13] Recloux, I., et al. “Active and Passive Protection of AA2024-T3 by a Hybrid Inhibitor Doped Mesoporous Sol–Gel and Top Coating System.” *Surface and Coatings Technology*, vol. 303, 2016, pp. 352–361., doi:10.1016/j.surfcoat.2015.11.002.

[14] Taryba, M.g., et al. “Novel Use of a Micro-Optode in Overcoming the Negative Influence of the Amperometric Micro-Probe on Localized Corrosion Measurements.” *Corrosion Science*, vol. 95, 2015, pp. 1–5., doi:10.1016/j.corsci.2015.02.037.

[15] Alodan, Maher A. “Detection of Localized Corrosion of Aluminum Alloys Using Fluorescence Microscopy.” *Journal of The Electrochemical Society*, vol. 145, no. 5, 1998, p. 1571., doi:10.1149/1.1838520.

[16] Lee, Woo-Jin, et al. “Analysis of Products at Reaction Sites by Fluorescence Microspectroscopy Using the f-NSOM Technique.” *Journal of The Electrochemical Society*, vol. 152, no. 3, 2005, doi:10.1149/1.1859816.

[17] Silva, Eduardo L., et al. “The Reduction of Dissolved Oxygen During Magnesium Corrosion.” *ChemistryOpen*, vol. 7, no. 8, 2018, pp. 664–668., doi:10.1002/open.201800076.

[18] Dolgikh, Olga, et al. “Corrosion Protection of Steel Cut-Edges by Hot-Dip Galvanized Al(Zn,Mg) Coatings in 1 Wt% NaCl: Part II. Numerical Simulations.” *Materials and Corrosion*, vol. 70, no. 5, Feb. 2019, pp. 780–792., doi:10.1002/maco.201810210.

[19] Topa, V., et al. “A Transient Multi-Ion Transport Model for Galvanized Steel Corrosion Protection.” *Electrochimica Acta*, vol. 77, 2012, pp. 339–347., doi:10.1016/j.electacta.2012.06.021.

[20] Dolgikh, O., et al. “Influence of the Electrolyte Film Thickness and NaCl Concentration on the Oxygen Reduction Current on Platinum.” *Corrosion Science*, vol. 102, 2016, pp. 338–347., doi:10.1016/j.corsci.2015.10.025.

[21] Lamaka, S.v., et al. “Quasi-Simultaneous Measurements of Ionic Currents by Vibrating Probe and PH Distribution by Ion-Selective Microelectrode.” *Electrochemistry Communications*, vol. 13, no. 1, 2011, pp. 20–23., doi:10.1016/j.elecom.2010.11.002.

[22] Adey, Ra, and Sm Niku. “Computer Modelling of Galvanic Corrosion.” *ASTM Special Technical Publication*, 1988, pp. 96–117., doi:10.1520/stp26193s.

[23] Jia, J. X., et al. “Experimental Measurement and Computer Simulation of Galvanic Corrosion of Magnesium Coupled to Steel.” *Advanced Engineering Materials*, vol. 9, no. 1-2, 2007, pp. 65–74., doi:10.1002/adem.200600206.

[24] Thébault, F., et al. “Modeling Bimetallic Corrosion under Thin Electrolyte Films.” *Corrosion Science*, vol. 53, no. 1, 2011, pp. 201–207., doi:10.1016/j.corsci.2010.09.010.

[25] Murer, Nicolas, et al. “Numerical Modelling of the Galvanic Coupling in Aluminium Alloys: A Discussion on the Application of Local Probe Techniques.” *Corrosion Science*, vol. 52, no. 1, 2010, pp. 130–139., doi:10.1016/j.corsci.2009.08.051.

[26] Verbrugge, Mark. “Galvanic Corrosion over a Semi-Infinite, Planar Surface.” *Corrosion Science*, vol. 48, no. 11, 2006, pp. 3489–3512., doi:10.1016/j.corsci.2006.02.004.